World Meteorological Organization
Organisation météorologique mondiale

Secrétariat
7 bis, avenue de la Paix – Case postale 2300 – CH 1211 Genève 2 – Suisse
Tél.: +41 (0) 22 730 81 11 – Fax: +41 (0) 22 730 81 81
wmo@wmo.int – www.wmo.int

Weather • Climate • Water
Temps • Climat • Eau

MeteoSwiss Payerne CIMO Testbed
2013 report

Terms of Reference for CIMO Testbeds and Lead Centres are available under:
ttp://www.wmo.int/pages/prog/www/IMOP/Testbeds-and-LC.html

Name of Testbed / Lead Centre	**MeteoSwiss Payerne Testbed**
Location of Testbed / Lead Centre	**Payerne, Switzerland**

Contact Person for the Testbed/Lead Centre	
Courtesy Title	Dr
Family name	**Ruffieux**
First name	**Dominique**
Full Postal Address	**MeteoSwiss, Ch de l'Observatoire, 1530 Payerne, Switzerland**
Country	**Switzerland**
Tel. number(s)	**+41 26 662 6247**
Fax number(s)	**+41 26 662 6212**
Email(s)	**Dominique.ruffieux@meteoswiss.ch**
Has contact person changed in last 2 years?	Yes / No ? NO
If yes, who was the previous contact person?	

Report on Activities

1. Radiosounding (Rolf Philipona)

Significant differences of daytime temperature measurements observed during the 8th WMO Intercomparison of High Quality Radiosonde Systems held in Yangjiang, China, in July 2010, led us to reanalyze the radiation error of the Meteolabor SRS-C34 radiosonde.

On atmospheric air temperature measurements the radiation error changes with altitude, first due to changing radiative fluxes, and second due to decreasing pressure, and hence decreasing convective-conductive heat transfer between the sensor and the air. Many methods have been used to improve air temperature measurements. However, the most generally accepted, i.e., reducing the size of the sensor, reducing the surface emissivity/absorptivity and increasing the speed of the gas over the sensor, are to this day always a compromise and only partially eliminate the error.

In our experiments we used the Meteolabor thermocouple temperature sensor, which to our knowledge is smaller than all other temperature sensors presently used on operational radiosondes. As on most other radiosonde systems we have only limited knowledge on the emissivity/absorptivity of the sensor head and the connecting wires, for shortwave as well as longwave radiation. The ascent rate of the radiosonde during the experiments, and hence the ventilation, was the same as during standard operational radiosonde ascents. However, we measured the solar and thermal radiation fluxes downward and upward (see last report) and measured the air temperature under sun shaded and unshaded conditions during the same flight (Figure 1). This allowed us to directly measure the radiation error and relate it to the measured thermal and direct solar radiation.

Figure 1. Meteolabor SRS-C34 radiosonde with shading plate and thermocouple temperature sensors on both sides (left). Radiosonde package to measure radiation profiles and air temperature under shaded and unshaded conditions (right).

The basic idea is to measure air temperature during special radiosonde ascents with the operational all-time sun exposed sensor, and to compare these measurements with identical air sensors which are at times unshaded and at times shaded by a shading plate mounted on the radiosonde.

Data measured during a more or less cloud-free noontime flight is shown as an example in Figure 2. To explain the measurement principle we show the temperature measured by four sensors between 25 and 26 km altitude (left graph). Two operational all-time sun exposed temperature measurements from two different Meteolabor sondes TA3 C34/68 (blue) and TA3 C34/69 (green) show the uncorrected air temperature with an average difference of about 0.2 °C between the two sondes. T1 C34/69 (yellow) is one of the sensors which is located at a distance of 5 cm from the center of the shading plate. Between 25.1 and 25.5 km T1 C34/69 is about 0.8 °C colder than the operational sun exposed TA3 C34/69 sensor (both sensors are of the same sonde C34/69). Here we observe that during this phase T1 C34/69 was mostly shaded by the shading plate. Above 25.5 km we observe that T1 C34/69 is getting warmer than TA3 C34/69, hence during this phase the sensor is unshaded. From these measurements we conclude that the temperature measured by T1 C34/69 is the real true temperature reading, whenever the sensor is shaded by the plate. The red curve is the solar radiation corrected temperature measured by the Vaisala RS92-SGP sonde. We observe that around 25.2 km when T1 C34/69 is shaded, the RS92-SGP shows about 0.2 °C colder. The measurements also show that the sonde rotation (which is the same for all sondes) produces larger temperature variations on the Vaisala RS92-SGP than on the two Meteolabor TA3 sensors.

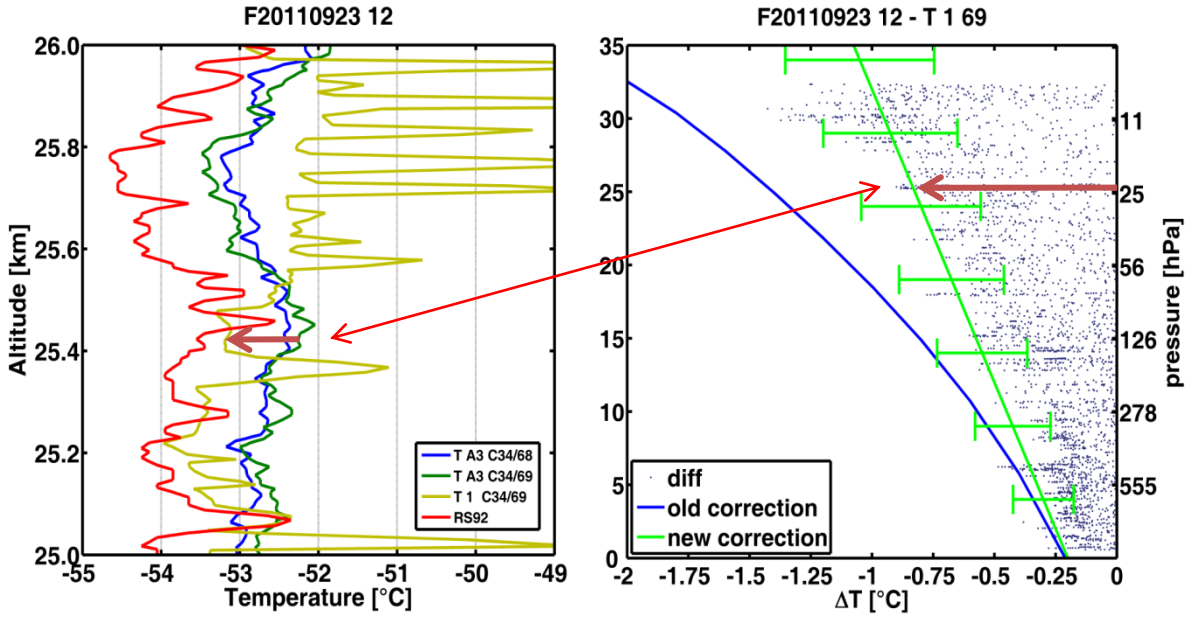

Figure 2. Measurements of four temperature sensors between 25 and 26 km altitude (left). Difference of T1 C34/69 minus TA3 C34/69 for all altitudes (right). The old (blue) and the new (green) radiation correction curves are shown.

The analysis over the entire altitude range is made by calculating the difference between the shaded T1 C34/69 measurement minus the sun exposed TA3 C34/69 measurement (red arrow on left graph). These differences are shown in Figure 2 right, with dots representing measurements taken each second when T1 was colder than TA3. The coldest temperatures measured under shaded conditions are then assumed to represent the correct air temperature measurement. The figure shows that the old solar radiation error curve (blue polynomial curve) is outside the blue dots, and hence too large particularly in the stratosphere. A new solar radiation error curve (green linear line) has therefore been determined, using measurements from 16 sensors, which were shaded/unshaded during 8 individual flights (Figure 3). The new curve represents an average solar error, following the coldest temperatures observed during the 16 measurements, and assuming a linear increase and an uncertainty of ± 0.1 °C at the surface and ± 0.3 °C at 32 km altitude. The uncertainty is based on the variations over the 16 measurements, which were made under different atmospheric conditions. In the troposphere the uncertainty is strongly influenced by varying cloud conditions and in the stratosphere it strongly depends on the reflection of the clouds below.

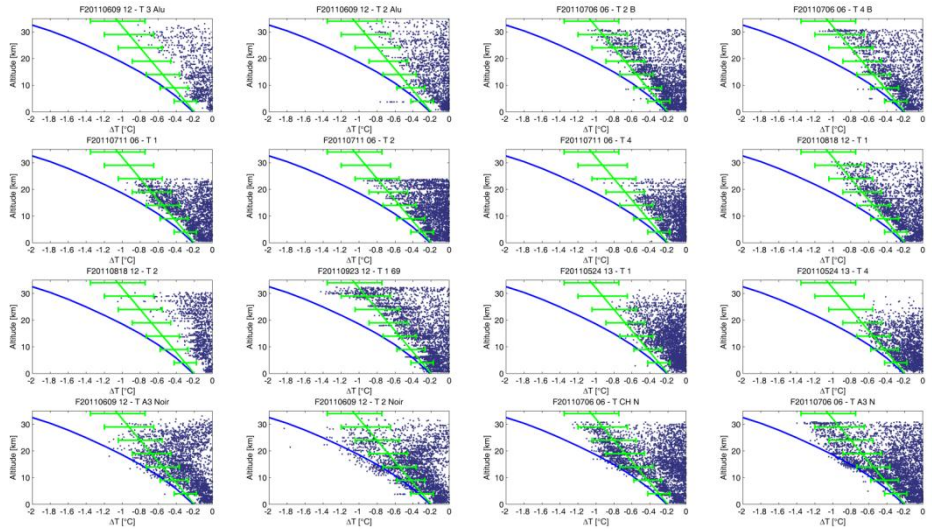

Figure 3. Temperature difference between shaded sensors located close to the shading plate minus unshaded temperature sensor, during eight individual flights (blue dots). The green line curve represents the new radiation correction curve. The old correction curve is shown in blue.

The old radiation error curve (blue) was calculated with respect to atmospheric pressure as a mean temperature difference ΔT_{year} profile for the whole year, and was represented by the second-degree polynomial fit:

$$\Delta T_{year}=2.927-1.293*\log(p)+0.131*(\log(p))^2 \quad (1)$$

The new radiation error curve (green) or mean temperature difference ΔT_{year} profile for the whole year on the other hand, is represented as a first order linear equation with respect to geopotential altitude:

$$\Delta T_{year}=0.2+(0.8*(\text{Alt geo})/32'000) \quad (2)$$

Equation (2) is now used for the radiation correction of all UT12:00 noon flights made with the new digital Meteolabor SRS-C34 radiosonde at Payerne. The equation has also been used to correct all measurements made with the SRS-C34, since its introduction as operational radiosonde in January 2011.

The solar radiation error curves are applied on the daytime measurements of the 2010 WMO intercomparison results shown in Figure 4 left. The old radiation error curve (green) shows a strong cold bias, whereas the new curve (blue) better agrees with the measurements of the other sondes. Figure 4 right shows the 2010 WMO intercomparison results referenced to Meteolabor results, which are corrected with the new solar radiation error curve. In the lower troposphere the measurements of all radiosonde systems are -0.2 ±0.2 °C colder than Meteolabor measurements, which is likely due to solar and thermal radiation errors. However, in the stratosphere the new radiation correction centers the Meteolabor results within the results of the majority of the other radiosonde systems. The differences in the troposphere will have to be further analyzed and future international intercomparisons will help to reduce differences between radiosonde temperature measurements. More details on these investigations can be found in Philipona et al., JTECH 2013.

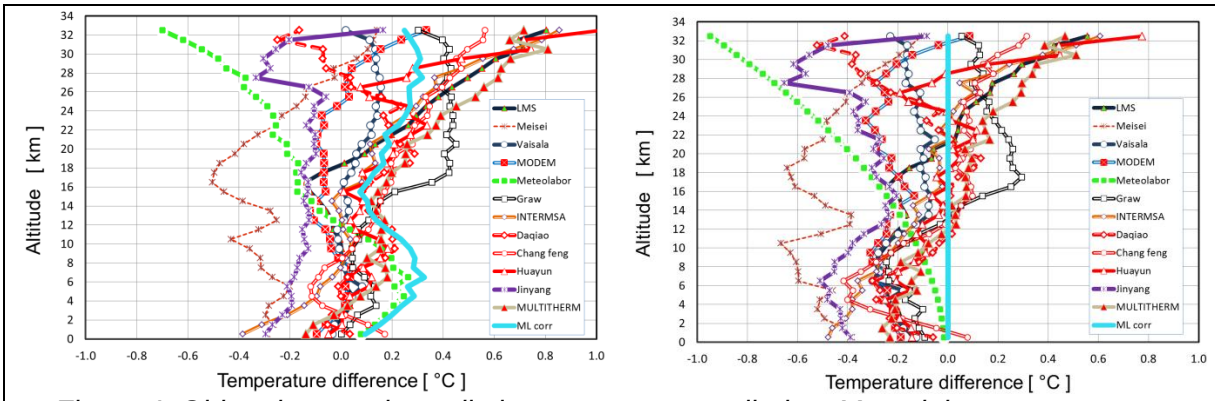

Figure 4. Old and new solar radiation error curve applied on Meteolabor measurements taken during the 2010 WMO radiosonde intercomparisons in China (left). WMO intercomparison results referenced to new Meteolabor radiation error curve (right).

Reference:
R. Philipona, A. Kräuchi, G. Romanens, G. Levrat, P. Ruppert, E. Brocard, P. Jeannet, D. Ruffieux, B. Calpini : Solar and Thermal Radiation Errors on Upper-Air Radiosonde Temperature Measurements. Journal of Atmospheric and Oceanic Technology, **30**, 2382, 2013, DOI: 10.1175/JTECH-D-13-00047.1.

2. Ground-based remote sensing (Alexander Haefele)

Raman lidar

The Raman lidar deployed at the Payerne site since 2008 is designed to measure of humidity, temperature and aerosols profiles for operational meteorology and for long term observations of high quality. A big effort has been made to make the system fully automatic and to achieve a data availability of more than 50% on the basis of several years.

The water vapor data have been reprocessed using only night time data and long integration times of several hours. In this configuration water vapor profiles can be retrieved covering the upper troposphere (UT) in summer as well as in winter. The UT water vapor measurements have been validated against RS92 (Vaisala) and SnowWhite (Meteolabor) and agree with the reference measurements withing 10% up to 14 km (Figure 5).

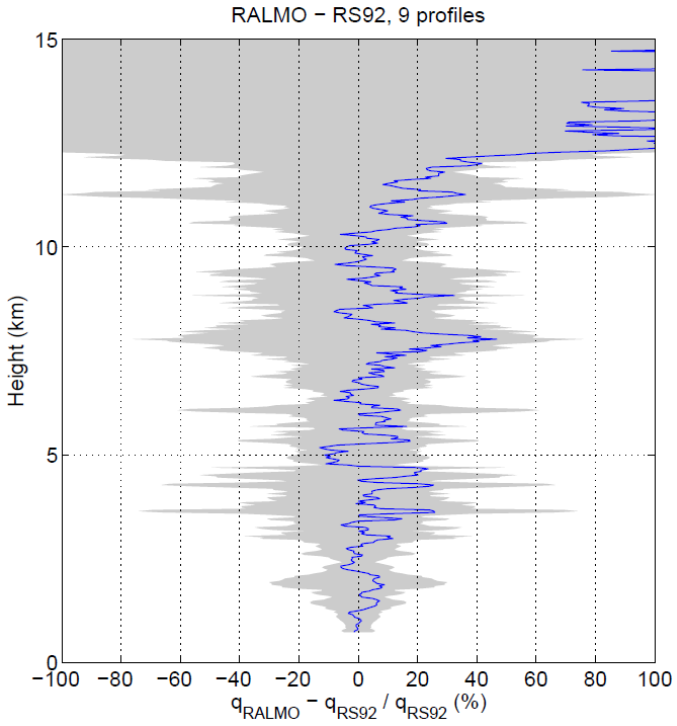

Figure 5. Mean (blue) and standard deviation (grey) of the difference between Raman lidar (RALMO) and RS92. The comparison is based on 9 nighttime profiles.

In October 2013 Shlomo Fastig from Soreq, Israel, joinded the lidar team at MeteoSwiss and EPFL in the frame of a sabbatical leave for one year. His project is

- to implement a system for improved calibration of the water vapor measurements based on a reference lamp
- to implement new acquisition channels for temperature and aerosol measurements.
- to develop and test a new design for the laser heads to improve system stability and reliability.

Results of these activities will be available during 2014.

Combination of ozone radiosonde and microwave radiometer

Routine ozone measurements are carried out at Payerne with ECC radiosondes and with a microwave radiometer. Ozone soundings are performed three times a week covering the altitude range from the surface to 35 km while an ozone profile between 20 and 60 km can be retrieved continuously every 30 min from the microwave measurements. To make an optimal use of these measurements and to retrieve calculate a combined profile that reaches from the surface up to 60 km the radiosounding is used as a priori information in the optimal estimation retrieval. A full characterization of the resulting profile including uncertainties has been made. It could be shown that in the middle and upper stratosphere the combined profile is in better agreement with reference instruments (Aura/MLS) than the microwave measurement alone. The figure 6 shows an illustration of the combined ozone profile.

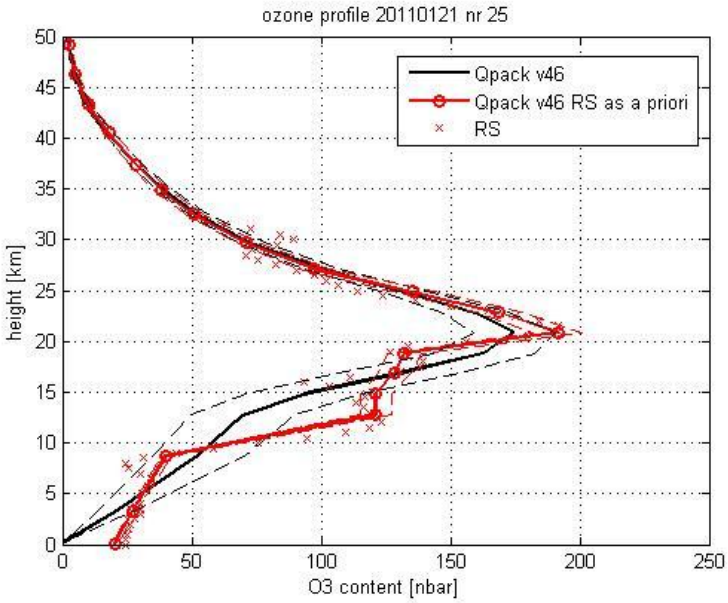

Figure 6. Combined ozone profile between the surface and 50 km using the radiosounging as a priori information in the optimal estimation retrieval. Below 20 km the information is coming mainly from the radiosounding and above from the microwave measurements.

Evaluation of a CHM15k lidar ceilometer

In the last years it has been realized that the new generation of ceilometers can not only provide cloud base height but also valuable information of the vertical distribution of aerosols. After the eruption of the Eyjafjellajökull volcano in 2010 the ashes have been detected at several sites with advanced ceilometers. Given the relatively low costs and the consequently high density of these instruments, ceilometers have a big potential in the field of aerosol monitoring in the boundary layer and the free troposphere. At Payerne a CHM15k ceilometer has been evaluated and compared with the Raman lidar. It could be shown in several cases that aerosols of different origins (Saharan dust, biomass burning, …) can be detected in the free troposphere allowing the determination of the lower and upper boundary of the layer. The figure 7 illustrates the capacities for aerosol profiling of the ceilometer. Calibration of ceilometers is an important step towards data harmonization and quantitative interpretation of the data. In the frame of the EUMETNET program E-PROFILE and the COST action TOPROF calibration procedures are being developed and validated.

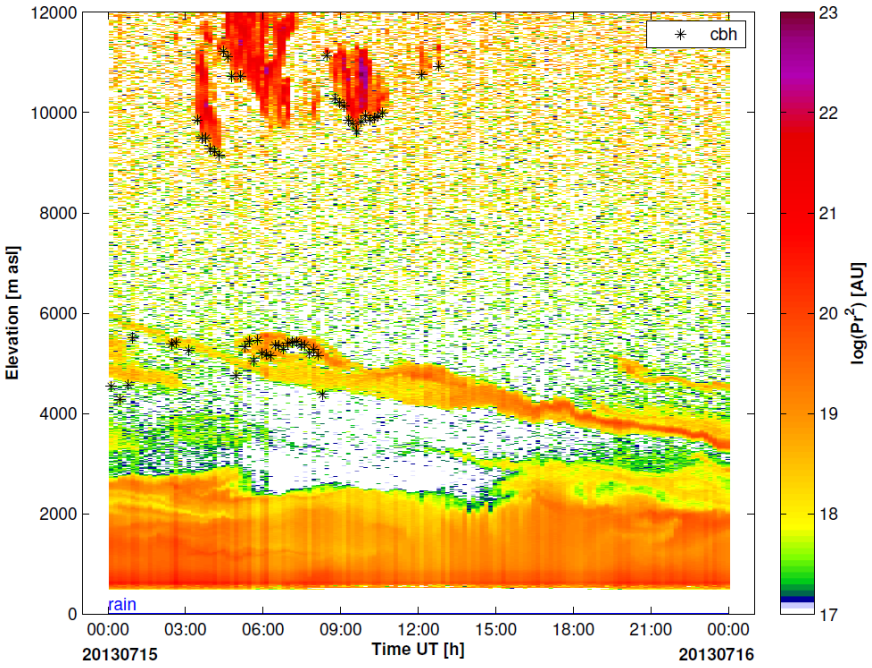

Figure 7. Detection of smoke particles from forest fires by a CHM15k above Payerne, Switzerland. The particles have been transported from Canada to Europe within 6 days. Erroneous cloud detection on the aerosol layer is occurs at around 06h UT between 4 and 6 km.

Operational estimation of the planetary boundary layer

The planetary boundary layer height (PBL height) is an important parameter for air quality and the dispersion of pollutants in the atmosphere. four different algorithms have been applied to remotely sensed temperature, humidity, wind and aerosol profiles for a continuous monitoring of the boundary layer. The results of these estimations of the PBL height have been compared to standard methods based on radiosoundings of temperature, humidity and wind. The PBL heights derived from remote sensing measurements agree on average within +/- 75 m with the PBL heights derived from radiosoundings. A publication of these results is in preparation. The four tested algorithms have been implemented in an operational tool for the aerological site of Payerne and for the two upper air sites Grenchen and Schaffhausen and provide real time PBL heights. An example of the PBL monitoring tool is shown in Figure 8.

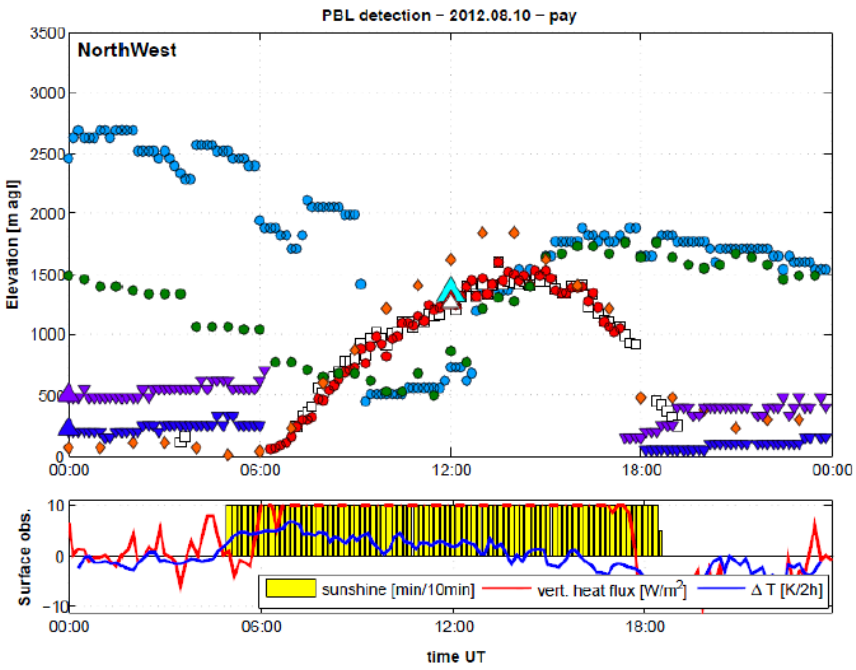

Figure 8. Example of the real time monitoring tool for the boundary layer height. For more information see publication (in preparation).

3. Performance evaluation of radiation sensors for the solar energy sector (Laurent Vuilleumier)

In the 2012 report, a contribution for evaluating the performance of radiometers designed for the solar energy sector was described. This was an effort to better understand the performance of these instrument within an emerging “regulatory” framework (e.g., standard operating procedures, certification, traceability, etc.) for such monitoring**.**

This activity included the organization by MeteoSwiss of an inter-comparison of radiometers measuring Direct Normal solar Irradiance (DNI) from 15/06/2012 to 15/09/2013. The goal was comparing target instruments to high accuracy radiation monitoring instruments (references) from the Baseline Surface Radiation Network (BSRN) Payerne site.

The target instruments allow the inference of the diffuse and direct component of solar (shortwave) radiation separately, and they should operate in a robust and cost effective way without the use of sun trackers and maintenance-intensive sensors: they are usually deployed in the field for continuous operation with limited maintenance.

The data analysis concerning this activity is still on-going. Preliminary results can be given first concerning the accuracy of the reference instruments, second concerning the general performance of the evaluated (target) instruments. A manuscript is in preparation for describing the accuracy of the reference instruments, and at least one other manuscript is in preparation for describing the performance evaluation of the radiometers designed for the solar energy sector.

Payerne BSRN reference data accuracy

Accuracy of reference measurements from the Payerne BSRN station is guaranteed by traceability of the instruments to standards and by observance of BSRN standard operating procedures. In addition strict quality control checks and quality analysis allow detecting instrumental malfunctions and evaluating the probability of instrumental drift.

The accuracy performances achieved using the such standard operating procedures and applying the quality control and quality assurance procedures were never fully evaluated. This inter-comparison prompted such an analysis and its preliminary results are summarized below. The uncertainty of broadband SW radiation monitoring were determined for Direct Normal Irradiance (DNI), Diffuse Horizontal Irradiance (DfHI) and Global Horizontal Irradiance (GHI). The analysis used data obtained with the best available technology as mandated by BSRN. It includes uncertainty sources that reflect realistic long-term operation conditions. In this study, 15 months of data were analyzed (15/06/2012-15/09/2013).

The uncertainties were first derived from the measurement equations according to the GUM methodology [1]. In a second step, redundant determinations of DNI, DfHI and GHI were used to verify that the differences between redundant observations are compatible with the uncertainties. Third, the signature of some uncertainty sources were sought within the error statistics to find out if corrections can be applied and what their effect is.

Table 1 summarizes the uncertainties determined in this study. The first two columns are uncertainties affecting the instruments' sensitivities with first the calibration uncertainty, and then the combined sensitivity uncertainty including sources such as non-linearity, temperature dependence, and aging. The following four columns are for uncertainty sources typical of long-term operational monitoring that are usually not indicated in manufacturer instrument specifications, except for the thermal effects. In addition to the latter, they include leveling, soiling and uncertainty due to the data acquisition electronics. Finally, the two last columns indicate the combined uncertainties including the sources described above. Since many uncertainties are proportional to the measured signal, combined uncertainties are computed for a small signal (50 Wm^{-2}, column 7) and a large signal (1000 Wm^{-2} for DNI and GHI, and 500 Wm^{-2} for DfHI, column 8).

Both standard and expanded uncertainties are given. The factors for converting one to the other are 1.96 when the uncertainties were mainly determined through a statistical analysis (assuming normal distribution) and $\sqrt{3}$ in other cases (assuming rectangular distribution). For some uncertainty sources, correction methods were applied and their effect estimated in this study. In such cases, the uncertainties are estimated both with and without the correction. There are also cases where the uncertainties were estimated as negligible either because the source does not apply to a given parameter or because it is was confirmed to be negligible. In Table 1 these uncertainties are indicated as ~0. For DfHI and GHI, several instruments are used, which implies several calibration uncertainties. The largest relative calibration uncertainties are given (worst case scenario). The last column gives the BSRN uncertainty targets [2]. The combined uncertainties (columns 6 and 7) are compared to the targets and the expanded uncertainties exceeding the targets are shown in red, the ones close to the target in orange and those satisfying the target are shown in green. Some table cells have a light red background. For these cells the analysis is not finished and the results are not given or preliminary.

		Sensitivity		Operational				Combined [b]		BSRN 2004 target
		calibration	combined [a]	thermal effect	leveling	soiling	data acquisition	small signal	large signal	
Direct (DNI)	no corr st	0.58%	0.72%	~0	~0	< 0.25%	0.06% + ~25µV	3.0 Wm^{-2}	7.8 Wm^{-2}	0.5% or 1.5 Wm^{-2}
	no corr ex	1.14%	1.41%			< 0.40%	0.1%+40µV	5.8 Wm^{-2}	15.3 Wm^{-2}	
	corr std		~0.6%					3.0 Wm^{-2}	7.2 Wm^{-2}	
	corr exp		~1%					5.8 Wm^{-2}	14.0 Wm^{-2}	
Diffuse (DfHI)	no corr st	≤ 0.69%	≤ 0.95%	~3 Wm^{-2}	~0	~0	0.06% + ~25µV	4.0 Wm^{-2}	6.0 Wm^{-2}	2% or 3 Wm^{-2}
	no corr ex	≤ 1.35%	≤ 1.87%	~6 Wm^{-2}			0.1%+40µV	7.9 Wm^{-2}	11.7 Wm^{-2}	
	corr std		~0.7%	~1 Wm^{-2}				2.9 Wm^{-2}	4.5 Wm^{-2}	
	corr exp		~1.4%	~2 Wm^{-2}				5.6 Wm^{-2}	8.8 Wm^{-2}	
Global (GHI)	no corr st	≤ 0.69%	≤ 0.95%	~3 Wm^{-2}		~0	0.06% + ~25µV	6.9 Wm^{-2}	11.2 Wm^{-2}	2% or 5 Wm^{-2}
	no corr ex	≤ 1.35%	≤ 1.87%	~6 Wm^{-2}			0.1%+40µV	13.5 Wm^{-2}	21.9 Wm^{-2}	
	corr std		~0.6%	~2 Wm^{-2}				6.5 Wm^{-2}	8.9 Wm^{-2}	
	corr exp		~1%	~4 Wm^{-2}				12.7 Wm^{-2}	17.4 Wm^{-2}	

Table 1. Uncertainties affecting SW measurements at the Payerne BSRN station. The two first columns give uncertainties for instrument sensitivities. The four next columns are related to operational uncertainties. The two next columns are for the combined uncertainties, and the last column gives the BSRN uncertainty targets. The uncertainties are given for DNI, DfHI and DrHI. In each case, the standard and expanded uncertainties are given, and in case a correction method was devised in the DNI inter-comparison analysis, an estimate of the uncertainty after correction is given. The combined uncertainties are computed for a small or a large signal, and the expanded combined uncertainties are compared to the BSRN targets; they are given in red when the target is not reached, in orange when close to the target, and in green when the target is reached.

[a] including calibration, non-linearity, sensitivity temperature dependence, aging, but not tilt.
[b] small signal is 50 Wm^{-2}; large signal is 1000 Wm^{-2} for global and 500 Wm^{-2} for diffuse.

The GHI and DfHI uncertainties range from 1.7% to 2.3%, and they satisfy or are close to the BSRN uncertainty targets for large signals. For small signals, the targets are not achieved and this is mainly because of the uncertainty from the data acquisition electronics, which is the factor where the most important accuracy gain could be achieved here. Some DAQ systems have lower uncertainty, but a DAQ system standardization was sought at MeteoSwiss for efficiency reason. The problem is under investigation and a solution using a high-accuracy pre-amplification level is sought for thermopile-based instruments.

The DNI uncertainty is ~1.5%, a factor 3 to 4 higher than the BSRN uncertainty target. In this case also an accuracy gain could be achieved at the DAQ level, but even without considering the DAQ uncertainty, the target is exceeded by a factor more than two. Even using an absolute cavity radiometer as transfer standard does not allow to reduce the uncertainty of the instrument sensitivity below ~1%. The BSRN DNI accuracy target is probably not achievable with the current

best available technology.

Evaluated instrument performances

The target instruments (Table 2) all measured the global irradiance and its components at 1-min time resolution. These can be compared to the reference BSRN measurements. The data availability is in average greater than 95%. The analysis of the comparisons is currently on-going and results reported here are preliminary.

Instrument provider	Instrument name	Number of instruments
Delta-T Devices Ltd	Sunshine Pyranometer (DELTA)	3
CSP Services GmbH	Rotating Shadowband Irradiometer (RSI)	2
Solar Millennium AG (through CSP Services)	Rotating Shadowband Pyranometer (RSP)	2
Irradiance Inc.	Rotating Shadowband Radiometer (IRR)	2

Table 2. List of target instruments participating to the inter-comparison.

Only data with sun elevation (θe) greater than 4° were included in the evaluation. To assess the instrument performance under specific conditions, the dataset was subdivided using different selection criteria. The first criterion is the sun elevation with on low sun elevation subset ($4° < \theta_e \leq 30°$), and a high sun elevation subset ($30° < \theta_e$). The low θ_e subset includes morning and evening data in summer and the whole day in winter, while the high θ_e subset includes the rest of the data.

For discriminating between cloudy and clear sky situations (in the vicinity of the sun position), the temporal variability of DNI is used with and the criteria is as follows

- sunny (low variability): $|\Delta DNI / \Delta t| < 30 Wm^{-2} min^{-1}$
- cloudy (high variability): $|\Delta DNI / \Delta t| \geq 30 Wm^{-2} min^{-1}$

For very low sun elevations ($\theta e \leq$ ~11.5°) the variability limit was lowered to $10 Wm^{-2} min^{-1}$. Additionally it was requested that the low DNI variability condition was fulfilled for at least 15 consecutive minutes in order to qualify a period as sunny (low DNI variability). Combining the two criteria (sun elevation and DNI variability) resulted in 4 data subsets.

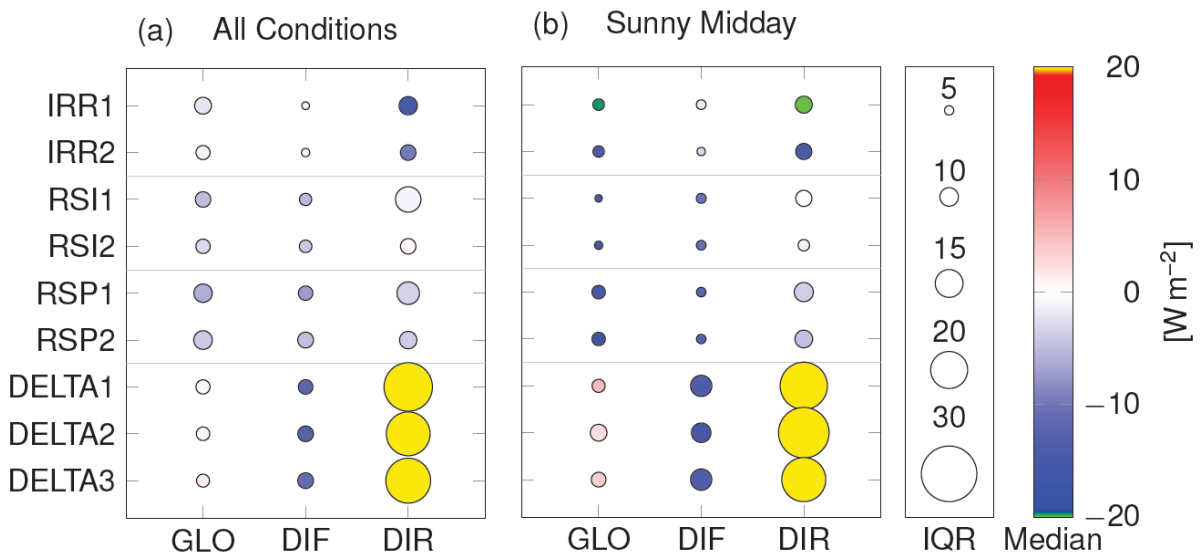

Figure 9. Summary of statistics (inter-quartile range and median bias) of errors (tested instrument measurement minus reference measurement) for SW global, diffuse and direct irradiance (GHI, DfHI and DNI), for all conditions (a) and for the subset at high sun elevation and low DNI variability (b), here designed as "sunny midday".

Figure 9a shows the median and interquartile range (IQR) for all tested instruments and components for all conditions, aggregated to one day. All instruments performed well for GHI with median bias between $-5.7 Wm^{-2}$ and $3 Wm^{-2}$ (IQR below $10 Wm^{-2}$). DfHI exhibits larger differences between the instrument types: the bias increases in absolute value (by chance) from the top of the figure (IRR: $\sim+0.5 Wm^{-2}$) to the bottom (DELTA instruments: $\sim-11 Wm^{-2}$). While having the best results for GHI and DfHI in terms of bias, the IRR instruments exhibit a strong bias for DNI ($-9 Wm^{-2}$ and $-16 Wm^{-2}$). Large DNI biases are also found for the three DELTAs ($\sim25 Wm^{-2}$), which also have the large IQR ($\sim25 Wm^{-2}$).

Figure 9b shows the same statistics but only for the subset with low DNI variability and high sun elevation. All shadow-band instruments have a larger median bias on the order of $-15 Wm^{-2}$ for GHI. The DELTAs have a similar bias as for all conditions ($\sim5.1 Wm^{-2}$). For DfHI, the IRRs show good performance ($\sim-3 Wm^{-2}$). All other instruments have bias around $-10 Wm^{-2}$ and $-15 Wm^{-2}$. For DNI, the performances of the RSIs and RSPs are good, the IRRs have larger negative bias, while the DELTAs exhibit large positive bias similar to the results for the whole dataset with again a significant variability (IQR $\sim25 Wm^{-2}$).

References cited

[1] Joint Committee for Guides in Metrology, Evaluation of measurement data — Guide to the expression of uncertainty in measurement, Bureau International des Poids et Mesures, Paris, 2008.

[2] McArthur, L. . J. B., 2005. Baseline Surface Radiation Network (BSRN) Operations Manual Version 2.1, s.l.: World Meteorological Organization (WMO/TD-No. 1274).

4. The SwissMetNet network and the CIMO SPICE experiment (Yves-Alain Roulet and Audrey Reverdin)

SwissMetNet

The renewal and extension of the ground-based meteorological network of MeteoSwiss, SwissMetNet, has entered its 3rd phase in 2012. Up to now about 100 full automatic stations have been built since 2004, and integrated into the SwissMetNet network (Figure 10), one unique platform for data acquisition and transfer.

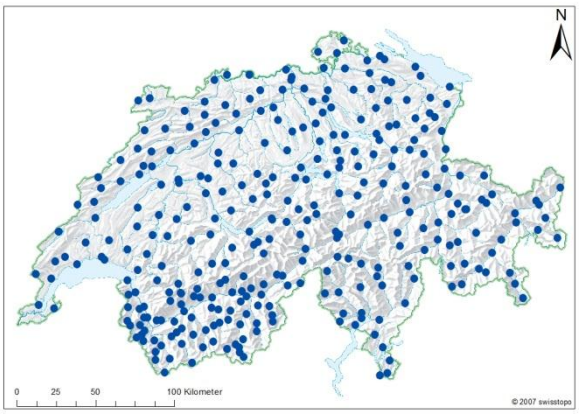

Figure 10. Final state of the SwissMetNet ground-based meteorological network.

A dedicated network for automatic precipitation measurement is currently being set up and added on SwissMetNet, for specific needs on severe weather monitoring and for automation of long series manual measurement. These compact and fast deployed stations use the Ott Pluvio2 rain gauge and a GPRS connection for data transmission. Not less than 120 stations will be built by 2014.

Recent developments on data acquisition and transfer performed at the CIMO Testbed in Payerne allowed to implement simple data logger on SwissMetNet (cost reduction, used for small stations like the precipitation stations), and to install the first station using satellite for data transfer (Figure 11).

Figure 11. SwissMetNet automatic precipitation station with data transfer via satellite.

CIMO SPICE

SPICE (Solid Precipitation Intercomparison Experiment) is a WMO/CIMO multi-sites intercomparison of instruments and systems of observation for the measurement of solid precipitation. One of the main objectives is the assessment of a wide range of instruments under various climates. For that purpose, around 20 sites worldwide are equipped and configured according to standards defined within the project, in order to allow comparison between the sites. The experiment started in October 2013 and is meant to last over two winter seasons.

At an elevation of 2500 m above sea level, the Weissfluhjoch (Davos, Switzerland) contains a SPICE site that has been set up by MeteoSwiss in close collaboration with the Swiss Institute for Snow and Avalanche Research (SLF), owner of the site, to provide reference measurements for the alpine climate (Figures 12 and 13). Among others, a reference set of instruments consisting of three Ott Pluvio^2 weighting gauges – one in a DFIR (Double Fence Intercomparison Reference), one with an Alter shield and one unshielded – will provide data sets for reference measurements analysis. A strong focus will be given to develop a methodology for precipitation phase discrimination using an optical disdrometer, and to link solid precipitation measurements with snow on the ground measurements using various manual and automatic methods.

Figure 12 : The SPICE reference site at Weissfluhjoch (Davos).

Figure 13 : The reference measurement : the DFIR with an OTT Pluvio^2 weighting gauge on his center and a disdrometer. Other instruments for temperature, humidity, wind give ancillary data around the gauge measurement.

Additional instruments under tests (provided by the manufacturers) are also installed, as for example precipitation gauges, precipitation laser monitor, GPS for snow on the ground, etc. Ancillary measurements (wind, temperature, pressure, humidity, solar radiation) are provided both from the SLF test site and from MeteoSwiss installations. A high resolution camera takes pictures of the gauges orifice. All collected data are transferred to the SPICE data base, being then available for data analysis, together with the other reference sites.

MeteoSwiss, as weather services of an alpine country, has a great interest in SPICE and its possible outcome. A strong effort (financial, HR) has been, and will be, put on this project (eg. construction of the DFIR, internship).

Main activities that TB/LC carried out in the last 2 years for which results will soon be available:

- SPICE experiment (see above)
- DNI Experiment (see above)
- Raman lidar measurements of upper tropospheric humidity: publication in preparation.
- Combined ozone profiles: publication in preparation.
- Ceilometer calibration and retrieval of optical aerosol parameters from Raman lidar: publication in preparation.
- Operational monitoring of planetary boundary layer: publication in preparation.

Which guidance documents/standard procedures were developed during the last 2 years (please include full reference and web-link if available)?

-
-
-

Which IOM reports / peer-reviewed publications were published in the last 2 years (please include full reference and web-link if available)?

R. Philipona, A. Kräuchi, G. Romanens, G. Levrat, P. Ruppert, E. Brocard, P. Jeannet, D. Ruffieux, B. Calpini : Solar and Thermal Radiation Errors on Upper-Air Radiosonde Temperature Measurements. Journal of Atmospheric and Oceanic Technology, **30**, 2382, 2013, DOI: 10.1175/JTECH-D-13-00047.1.

R. Philipona, A. Kräuchi, E. Brocard (2012) : Solar and thermal radiation profiles and radiative forcing measured through the atmosphere. Geophys. Res. Lett. , 39, L13806, doi: 10.1029/2012GL052087.

Dinoev, T. S., V. B. Simeonov, Y. F. Arshinov, S. M. Bobrovnikov, P. Ristori, B. Calpini, M. B. Parlange, and H. van den Bergh, Raman Lidar for Meteorological Observations, RALMO – Part I: Instrument description, Atmos. Meas. Tech. Discuss., 5, 6867-6914, 2012

Brocard, E., R. Philipona, A. Haefele, G. Romanens, D. Ruffieux, V. Simeonov, and B. Calpini, Raman Lidar for Meteorological Observations, RALMO – Part 2: Validation of water vapor measurements, Atmos. Meas. Tech. Discuss., 5, 6915-6948, 2012

Haefele A., E.- M. Barras, O. Maier, D. Ruffieux, and B. Calpini, Composite Temperature Profiles from Raman Lidar and Microwave Radiometer, Proceedings of the 9th International Symposium on Tropospheric Profiling, L'Aquila, Italy, 2012

Title(s) of IOM report(s) presently being developed by your Testbed/Lead Centre:
(please specify level of development: draft, ready for review, …)

-

Has your Testbed/Lead Centre collaborated with one or more CIMO Expert Teams in developing guidance material? Yes/No Yes

If yes, with which CIMO Expert Team(s)?

Strong relations were maintained with the Lindenberg DWD site for various GRUAN activities as well as with Table Mountain (USA) for Raman lidar activities

Capacity Building and Training Activities

Which capacity building/training activities have been carried out by the Testbed in the last 2 years?

- The main capacity building activities were related to the DNI Experiment (see above) during which a special workshop was organized
- A regular teaching activity (about once a year) is performed with staff from the Kenyan Meteorological Service (KMD) at Nairobi (radiosounding and Dobson)

Has your testbed developed a twinning activity / special relationship with a companion station/site from a developing country? Yes/No Yes

If yes, with which station/site?

A continuous collaboration is maintained between Meteoswiss and the Kenyan Meteorological Service (KMD) at Nairobi. The main focus of this partnership is the ozone measurements with both in-situ (radiosounding) and remote sensing (Dobson) ozone measurements

Is your Testbed/Lead Centre making an oral/poster presentation at this year's TECO? Yes / No
(If yes, please specify Title(s) and Author(s) of the presentation(s)) YES

- Y.-A. Roulet, J.-M. Aellen, S. Brönnimann, Ch. Fierz, J. Grandjean, B. Henchoz, Ch. Marty, A. Reverdin, M. Ruesch: REFERENCE MEASUREMENTS AT WEISSFLUHJOCH (SWITZERLAND) FOR THE WMO/CIMO SPICE PROJECT
- E. Maillard Barras, A. Haefele, R. Stübi: SITE ATMOSPHERIC STATE BEST ESTIMATE (SASBE) OF OZONE PROFILE ABOVE PAYERNE, SWITZERLAND: COMBINATION OF SIMULTANEOUS MICROWAVE RADIOMETER AND RADIOSONDE OZONE PROFILES
- A. Haefele, Dominique Ruffieux, Rolf Philipona: EVALUATION OF THE UNCERTAINTY BUDGET OF A BOUNDARY LAYER WIND PROFILER
- R. Philipona, A. Kräuchi, G. Romanens, G. Levrat, P. Ruppert, D. Ruffieux and B. Calpini : UPPER-AIR RADIOSONDE INTERCOMPARISONS AND UNCERTAINTY ESTIMATION
- M. Gabella, E. Morin, R. Notarpietro, M. Branca, A. Leunberger, U. Germann: HIGH SPATIO-TEMPORAL RESOLUTION OBSERVATIONS OF "HARD SCATTERERS" IN THE ATMOSPHERE AT 10GHZ: PRELIMINARY EXPERIENCES IN SEMI-ARID REGIONS AND IN THE WESTERN ALPS
- J. Klausen, B. Howe, and the ET-WDC and TT-WMD Team: METADATA FOR WIS AND WIGOS: GAWPROFILE OF ISO19115 AND DRAFT WIGOS CORE METADATA STANDARD

Recent Changes in Circumstance

Have there been any recent changes in your Test Bed/Lead Centre's capabilities? If so, please specify:

-
-
-

Have there been any recent changes in your Test Bed/Lead Centre's infrastructure? If so, please specify:

-
-

Have there been any recent changes in your staffing? If so, please specify, and advise whether replacement staff have the required competencies:

-
-

Future Plans

What are your plans for the next two years?

- Continuation of the efforts to develop Payerne as a GRUAN site
- Reinforcement of the lidar–related activities (both Raman lidar and ceilometers)
- Continuation of the DNI experiment
- Continuation of the SPICE experiment

Is your Testbed/Lead Centre able to continue in the role	Yes / No YES

of a Test Bed/Lead Centre during the coming two years?	

Other relevant information (other activities of special interest to CIMO, etc…)
• • •

24.02.2014	Dominique Ruffieux
Date	**Name of Person Filling the Form**